Proceedings of the 3rd
International Conference on Advanced Mechatronics
Okayama, JAPAN - Aug. 1998, JSME

Trajectory Formation of Human Arm with Nonholonomic Constraints

Yoshiyuki Tanaka Toshio Tsuji Makoto Kaneko
Faculty of Engineering, Hiroshima University
Higashi-Hiroshima, 739-8527 Japan

Abstract

In this paper, we focus on the manipulation of a holding nonholonomic toy car and attempt to generate similar trajectories to the human ones. In order to reveal what kind of trajectories a human generates, we first performed experiments with subjects. Then, it is shown that the generated hand velocity profiles can be classified into two classes: a single-peaked profile and a double-peaked one. By modeling these primitive profiles with the TBG, we try to generate the trajectory for the robots by the TBG based trajectory generation method. Finally, the results of computer simulations are shown and compared with the human trajectories
Key Words: Human movements, trajectory generation, nonholonomic constraints, potential field method, TBG.

1 Introduction

With the latest progress of robotic technology, it has been expected that an advanced type of robot being able to cowork and coexsit with a human will be developed and commonly used at home or a workspace in the near future. In fact, the development of the human-shaped robot which is called the humanoid robot has been actively performed [1], so that a friendly feeling of a human toward the robot is practically realized from a cosmetic point of view. However, no matter how similar to a human being in appearance the robot is, it will not be able to coexist with a human in a daily life if it cannot act or perform a task with human-like movements.

On the other hand, there have been many studies on a mechanism of human arm movements [2]-[6]. For instance, Morasso [2] measured reaching movements of the human two-joint arm restricted to an horizontal plane, and found the following common invariant kinematic features: When a subject was instructed merely to move his hand from one point to another, the hand usually moved along a roughly straight path with a bell-shaped velocity profile. As the explanation for the trajectory generation mechanism of this human arm movements, many models have been proposed; for example, "a minimum jerk model" [3], "a minimum torque-change model" [4] and "a VITE model" [5]. The first and the second models assert that the human trajectory generator is the feed-forward system, and the last one deals it as the feedback system. All of these models can generate hand trajectories in good agreement with experimental data.

Also, Morasso et al. [6] proposed a Time Base Generator (TBG) which generates a time-series with a bell-shaped velocity profile, and showed that a straight and a curved hand trajectory can be generated by synchronizing a translational and a rotational velocity of the hand with the TBG signal. Then, Tsuji et al. [7] [8] applied the TBG mechanism to the control of a non-holonomic robot and a redundant manipulator. Tanaka et al. [9] has developed a trajectory generation method based on the artificial potential field approach (APFA) with a combination of time scale transformation and the TBG, named "time scaled artificial potential field approach." These previous studies, however, have not dealt with any constraints in the hand movement, although a human movement is often constrained by environments on performing an ordinary work in a daily life.

In the present paper, we attempt to reproduce hand trajectories generated by a human in operating a nonholonomic-constrained task. The manipulation of a holding nonholonomic toy car from one point to another is chosen as the task. First, in order to reveal what kind of hand trajectories a human would generate for this task, the trajectory generation experiments with subjects are performed. Through the observation of human hand movements, it is shown that the generated hand velocity profiles can be classified into two classes: a single-peaked profile and a double-peaked one. By modeling these primitive profiles with the TBG on the basis of the experimental results, we try to generate the trajectory for the robots operating the same task.

This paper is organized as follows: Section 2 describes the trajectory generation experiments on the nonholonomic-constrained task. In section 3, a feedback controller to reproduce the observed human hand trajectories is designed by means of the time scaled artificial potential field approach. Finally, the results of computer simulations are shown and compared with the human trajectories in Section 4.

2 Trajectory formation of human arm

2.1 Experimental conditions

Figure 1 shows an experimental apparatus. A subject is instructed to sit on his heels and move the holding nonholonomic toy car which has two wheels and

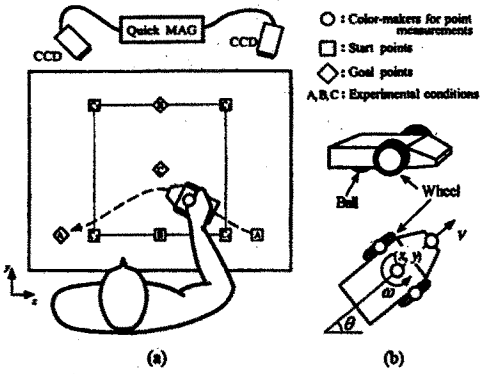

Fig.1 Experimental apparatus

one spherical wheel as shown in Fig. 1 (b) from an initial point marked with □ to a target point ◇ on a specified condition (see Fig. 1 (a)). In the experiment, the translational velocity v and the angular velocity ω of the toy car are calculated as human hand velocities by measuring the movements of the toy car and the subject's arm with a stereo camera system (Quick MAG, OUYOU KEISOKU KENKYUSYO INC.).

The camera system can detect a 3-D position of a color marker (marked with ○ in Fig. 1 (b)) attached at a point of measurement, maximum of 8 points, from two 2-D image sequences taken by two CCD cameras in real time. Both v and ω were calculated through the numeric derivation of the smoothed marker's positional data where the cut-off frequency of the second-order Butterworth filter is automatically determined by Winter's method [10]. With this apparatus, we carried out the following three kinds of experiments (see Fig. 1 (a)):

A: Move the toy car from the initial point [A] to the target point ◈ with the initial posture $\theta_0 = \pi$[rad] and the target posture $\theta_d = \pi$[rad] in the generalized coordinates Σ_b. Also, the subject is asked to generate a vertically curved spatial trajectory like the dotted line shown in Fig. 1 (a) as the trials goes on.

B: Move the toy car from the initial point [B] to the target point ◈ with the initial posture $\theta_0 = \frac{\pi}{2}$[rad] and the target posture $\theta_d = \frac{\pi}{2}$[rad] in the generalized coordinates Σ_b. The subject is asked to generate a horizontally curved spatial trajectory as the trials goes on.

C: Move the toy car from the initial points [C] ($i = 1, \cdots, 4$) to the target point ◈ under the initial posture $\theta_0 = \frac{\pi}{2}$[rad] and the target posture $\theta_d = \pi$[rad]. The initial points are located at the vartexes of a square whose sides are 400 [mm] long and the target point is positioned at the center of the square.

In the experiments, the number of subjects was three (male university students aged 22, 23 and 28), and the order of the experimental conditions and the number of trials were changed for each subject.

2.2 Generated spatio-temporal trajectories

Figure 2 shows a typical example of the observed spatial trajectories and translational velocity profiles of the toy car, where the translational velocity v is normalized by its maximum velocity v_{max} and the time t by the measured movement time t_f from a initial point to a target for each trials, respectively.

It can be seen that the straight trajectories have single-peaked velocity profiles which peaks around $t = t_f/2$ as shown in Fig. 2 (a),(b). Also, it should be noticed that as the amplitude of the curvature is lager, the velocity profile tends to be more sharply double-peaked.

On the other hand, under the experimental condition C, the subjects generated two kinds of spatial trajectories: a trajectory including one switching point, and a quadrantal arc. One of them were chosen according to the specified initial point as shown in Fig. 2 (c). It should be noticed that the quadrantal-arc trajectories have the single-peaked velocity profiles and the others the coupled-profiles with two single-peaked ones. From features of the generated switching trajectories, it can be suggested that a switching trajectory is produced as the result of connecting a straight line with a quadrantal arc at the switching point.

Summing up, we observed the following features of the human hand trajectories through the experiments:

1) The subjects generate two types of the primitive velocity profiles: a single-peaked profile and a double-peaked one.

2) The subjects generate the different spatial trajectories according to the initial point and the target one.

3) The subjects generate a velocity profile out of two primitive ones according to the generated spatial trajectory.

4) The straight trajectory generated by the subjects has a single-peaked velocity profile whether there exists the nonholonomic constraint on the hand movements in a given task or not.

3 Trajectory generation using Time Base Generator

In the previous section, the human primitive movements on the manipulation of the nonholonomic toy car was revealed. Here, we explain a method for generating a spatio-temporal trajectory which has similar features of the human movements observed in the experiments.

Tanaka et al. [9] have developed the trajectory generation method based on the artificial potential field approach with the combination of a time scale transformation and a time base generator (TBG) [6]. The TBG generates a bell-shaped velocity profile and works as a time scale compressor. The proposed method applied to the generation of spatio-temporal trajectories of a mobile robot and a manipulator. In this section, we use this method to reproduce the experimentally observed human hand trajectories.

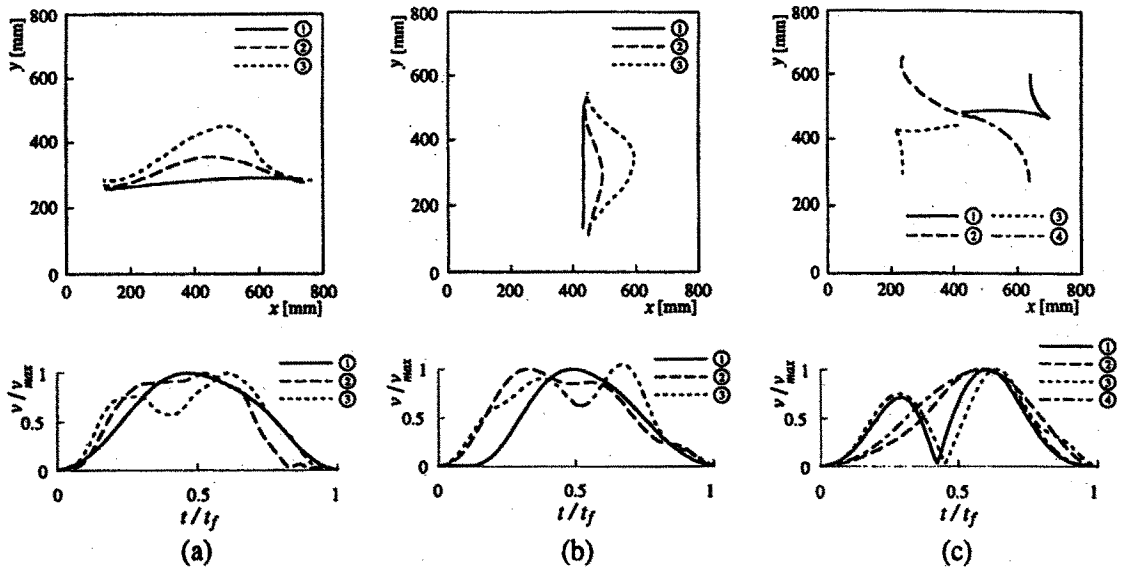

Fig.2 Generated spatio-temporal trajectories under the different experimental conditions

3.1 Virtual time and the TBG

First, we define a virtual time s for time scaling the system. The relationship between actual time t and virtual time s is given by

$$\frac{\mathrm{d}s}{\mathrm{d}t} = a(t)\,, \tag{1}$$

where the continuous function $a(t)$, called the time scale function [11], is defined as follows:

$$a(t) = -p\frac{\dot{\xi}}{\xi}\,, \tag{2}$$

where p is a positive constant and $\xi(t)$ is a non-increasing function generated by the Time Base Generator (TBG) [7] [8]. $\xi(t)$ has a bell-shaped velocity profile satisfying $\xi(0) = 1$ and $\xi(t_f) = 0$ with the convergence time t_f. The dynamics of ξ is defined as follows:

$$\dot{\xi} = -\gamma(\xi(1-\xi))^{\beta}, \tag{3}$$

where γ and β are positive constants under $0 < \beta < 1.0$. The convergence time t_f can be calculated with the gamma function $\Gamma(\,\cdot\,)$ as

$$t_f = \int_0^{t_f} dt = \int_1^0 \frac{\mathrm{d}\xi}{\dot{\xi}} = \frac{\Gamma^2(1-\beta)}{\gamma\Gamma(2-2\beta)}. \tag{4}$$

Figure 3 shows the time histories of ξ and $\dot{\xi}$ depending on convergence time $t_f = 1.0, 3.0, 5.0$ [s] under the parameter $\beta = 0.5$.

From (1) and (2), the virtual time s can be represented with respect to ξ as follows:

$$s = \int_0^t a(t)\,dt = -p\ln\xi(t)\,. \tag{5}$$

It is obvious that the virtual time s given in (5) never goes backward against the actual time t. This virtual time s is used as a new time scale in this paper.

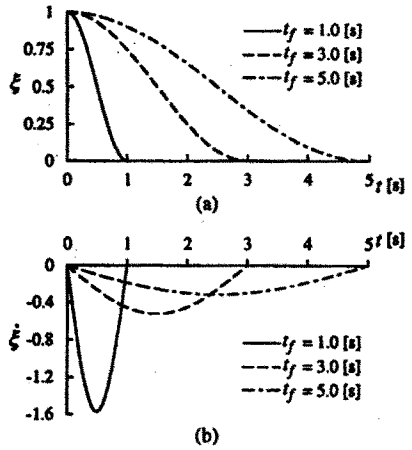

Fig.3 Dynamic behavior of the TBG

3.2 Time scaled artificial potential field approach

Generally, the kimenatics of the robot system can be described by

$$\dot{\boldsymbol{X}} = \boldsymbol{G}(\boldsymbol{X})\boldsymbol{U}, \tag{6}$$

where $\boldsymbol{X} \in \Re^n$ is the position vector of the robot; $\boldsymbol{U} \in \Re^n$ is the input vector; and it is assumed that $\det \boldsymbol{G}(\boldsymbol{X}) \neq 0$. The system given in (6) can be rewritten in the virtual time s defined by (5) as follows:

$$\frac{\mathrm{d}\boldsymbol{X}}{\mathrm{d}s} = \frac{\mathrm{d}\boldsymbol{X}}{\mathrm{d}t}\frac{\mathrm{d}t}{\mathrm{d}s} = \boldsymbol{G}(\boldsymbol{X})\boldsymbol{U}_s, \tag{7}$$

where

$$\boldsymbol{U}_s = \frac{1}{a(t)}\boldsymbol{U}. \tag{8}$$

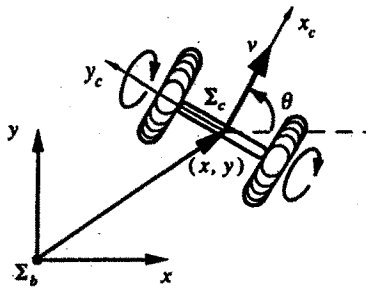

Fig.4 Model of a toy car with two wheels

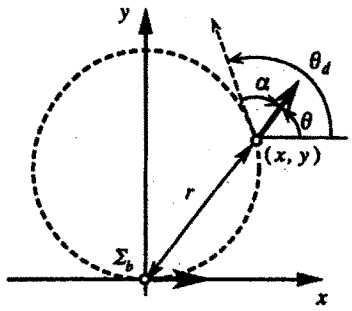

Fig.5 Coordinate transformation

On the other hand, in the artificial potential field approach (APFA) [7] [8], the goal is represented by an artificial attractive potential field which is created by the defined potential function $V(\boldsymbol{X})$. The potential function $V(\boldsymbol{X})$ has the minimum value $V(\boldsymbol{X}_d) = 0$ at the target point $\boldsymbol{X}_d$ in the task space, so that the trajectory to the target can be associated with the unique flow-line of the gradient field through the initial position and be generated via a flow-line tracking process. Through the inverse time-scale transformation from virtual time s to actual time t for the feedback controller $\boldsymbol{U}_s$ for the system (7) designed by APFA, the feedback control law $\boldsymbol{U}$ in actual time t is derived as

$$\boldsymbol{U} = -a(t)\boldsymbol{G}^{-1}(\boldsymbol{X})\frac{\partial V}{\partial \boldsymbol{X}}. \tag{9}$$

By means of the derived controller $\boldsymbol{U}$, the system (6) in the actual time scale can be stable to the equilibrium point at the specified time t_f. In this paper, we attempt to make the robots generate the trajectories which are similar to the observed human primitive movements by using the TBG based method.

3.3 Trajectory generation of a nonholonomic car

In this subsection, with the TBG based method, a feedback control law which can generate a spatio-temporal trajectory of the toy car is designed on the basis of the observed features of the experimental results with the subjects.

Figure 4 shows a model of the unicycle-like car which a subject manipulates in the experiment. Σ_b denotes the world coordinate system (for an operational space), and Σ_c is the moving coordinate system whose origin is set at the center of two wheels of the car and the x_c axis is oriented along the direction of motion of the car. Thus, we can choose the following generalized coordinates of the vehicle: position (x, y) and orientation angle θ of Σ_c with respect to Σ_b.

The kinematics of the car can be described by the following relationship between the time derivative $\boldsymbol{x} = (x, y, \theta)^T$ and the linear and the angular velocity of the car $\boldsymbol{u} = (v, \omega)^T$:

$$\dot{\boldsymbol{x}} = \boldsymbol{g}(\boldsymbol{x})\boldsymbol{u}, \tag{10}$$

where

$$\boldsymbol{g}(\boldsymbol{x}) = \begin{bmatrix} \cos\theta & 0 \\ \sin\theta & 0 \\ 0 & 1 \end{bmatrix}. \tag{11}$$

From the system equation (10), we can easily derive the following kinematic constraint [7]:

$$\dot{x}\sin\theta - \dot{y}\cos\theta = 0. \tag{12}$$

Therefore, there is the nonholonomic constraint given by (12) imposed on the hand movement of the subject in the process of manipulating the car.

In order to control the system, we adopt the piecewise smooth feedback control law proposed by Canudas de Wit and Sørdalen [12] which uses the family of circles that pass through the origin and the current position of the car and contact the x axis at the origin as shown in Fig. 5. In the figure, θ_d belonging to $[-\pi, \pi)$ represents the tangential direction of this circle at the position x.

Let α denote the angle between the tangential direction θ_d and the current angular orientation θ with the intention of designing a control law which can eliminate this kind of *orientation error* together with the corresponding *positional error* denoted by the distance r from the target. The following coordinate transformation from $\boldsymbol{x} = (x, y, \theta)^T$ to $\boldsymbol{z} = (r, \alpha)^T$ is then introduced [7]:

$$r(x, y) = \sqrt{x^2 + y^2}, \tag{13}$$

$$\alpha(x, y, \theta) = e + 2n(e)\pi, \tag{14}$$

$$e = \theta - \theta_d, \tag{15}$$

$$\theta_d = 2\mathrm{atan2}(y, x), \tag{16}$$

where $n(e)$ is a function that takes an integer in order to satisfy $\alpha \in [-\pi, \pi)$. Also, $\mathrm{atan2}(\cdot, \cdot)$ is the scalar function defined as $\mathrm{atan2}(a, b) = \arg(b + ja)$, where j denotes the imaginary unit and arg denotes the argument of a complex number. As a result, the current state of the car can be represented by

$$\boldsymbol{z} = F(\boldsymbol{x}) = \begin{bmatrix} r(x, y) \\ \alpha(x, y, \theta) \end{bmatrix} \tag{17}$$

and the target configuration of the car is transformed from $\boldsymbol{x}_d = (0, 0)^T$ to $\boldsymbol{z}_d = (0, 0)^T$.

Substituting (11) into the time derivation of equation (18), we have the relationship between $\dot{\boldsymbol{z}}$ and the system input $\boldsymbol{u}$:

$$\dot{\boldsymbol{z}} = \boldsymbol{J}(\boldsymbol{x})\boldsymbol{G}(\boldsymbol{x})\boldsymbol{u} = \boldsymbol{B}(\boldsymbol{x})\boldsymbol{u}, \tag{18}$$

where

$$J(x) = \begin{bmatrix} \frac{x}{\sqrt{(x^2+y^2)}} & -\frac{y}{\sqrt{(x^2+y^2)}} & 0 \\ \frac{2y}{x^2+y^2} & -\frac{2x}{x^2+y^2} & 1 \end{bmatrix}, \quad (19)$$

$$B(x) = \begin{bmatrix} b_1 & 0 \\ b_2 & 1 \end{bmatrix}, \quad (20)$$

$$b_1 = -\frac{1}{\sqrt{x^2+y^2}}(x\cos\theta + y\sin\theta), \quad (21)$$

$$b_2 = \frac{2}{x^2+y^2}(y\cos\theta - x\sin\theta). \quad (22)$$

It can be seen that the number of state variables is reduced to the same number as the system input. For this system, the following potential function V so as to design the feedback controller can be defined:

$$V = \frac{1}{2}\left(k_r r^2 + k_\alpha \alpha^2\right), \quad (23)$$

where k_r and k_α are positive constants.

From (9), we can design the feedback controller u based on the potential function V (23) as

$$u = -a(t)B^{-1}(x)\frac{\partial V}{\partial z} = \begin{bmatrix} \frac{pr\dot{\xi}}{2b_1\xi} \\ -b_2 v + \frac{p\alpha\dot{\xi}}{2\xi} \end{bmatrix}' \quad (24)$$

under the assumption of $\det B(x) \neq 0$ except at the target position x_d. With the feedback controller u, the time derivative of V yields

$$\dot{V} = \frac{\partial V}{\partial z}B(x)u = pV\frac{\dot{\xi}}{\xi} < 0. \quad (25)$$

As $\dot{V}$ is always negative except at the equilibrium point, the system of the car in the actual time scale is asymptotically stable by means of the designed feedback control law u. Moreover, this differential equation given in (25) can be readily solved as follows [8]:

$$V = V_0\xi^p, \quad (26)$$

where $V_0 = V(x_0)$ is the initial value of V. It can be seen that the potential function V is "synchronized" with the TBG because V is proportional to the pth power of ξ. Since ξ reaches zero at t_f so must do V: in other words, the car with two wheels is bound to reach the target position x_d from the initial position x_0 just at $t = t_f$ with the controller u.

4 Computer simulations

In this section, the observed-human-fundamental trajectories whose velocity profiles are single / double-peaked is reproduced by means of the designed controller (24). In the simulations explained below, the target posture is $\theta_d = \pi$ [rad] with the convergence time $t_f = 2.5$ [s] under the parameters $p = 2.0$, $\beta = 0.75$, $k_r = k_\alpha = 1.0$.

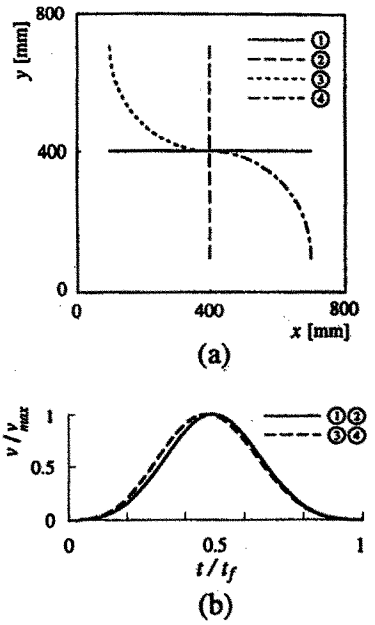

Fig.6 Generated trajectories with single-peaked velocity profiles

Table 1 Initial conditions and goal positions

	①	②	③	④
Initial point [m]	$(0.7, 0.4)^T$	$(0.4, 0.1)^T$	$(0.1, 0.7)^T$	$(0.7, 0.1)^T$
Goal point [m]	$(0.1, 0.4)^T$	$(0.4, 0.7)^T$	$(0.4, 0.4)^T$	$(0.4, 0.4)^T$
Initial posture [rad]	π	$\pi/2$	$\pi/2$	$\pi/2$

4.1 Generation of a single-peaked velocity profile

Figure 8 shows the generated spatio-temporal trajectories which have single-peaked velocity profiles with the different initial conditions (x_0, θ_0) and the target points x_d as shown in Table 1. In the time histories of the velocity (Fig. 6 (b)), the vertical axis is normalized by the maximum velocity v_{max} for each trial, and the horizontal axis by the specified time $t_f = 2.5$ [s], respectively. It can be seen that the generated spatial trajectories are straight lines or quadrantal arcs with single-peaked velocity profiles which take the maximum value at $t = \frac{t_f}{2}$. The designed controller can generate spatio-temporal trajectories which are similar to human primitive trajectories.

4.2 Generation of a double-peaked velocity profile

In order to generate a curved trajectory, we set a via-point x_v^* and a via-orientation $\theta_v^* = \mathrm{atan2}(y_v^*, x_v^*)$ in the task space, which moves to the targets from $t = t_i^a$ to $t = t_i^b$ $(i = x, y, \theta)$ smoothly.

Figure 9 shows the generated spatio-temporal trajectories with the initial position $(x_0, \theta_0) = (0.7$ [m], 0.4 [m], π [rad]$)^T$ and the target point $x_d = (0.1, 0.4)^T$ [m]. For the curved spatial trajectories ②, ③ in Fig. 7 (a), the via-points were set at $x_v^* = (0.4,\ 0.6)^T$,

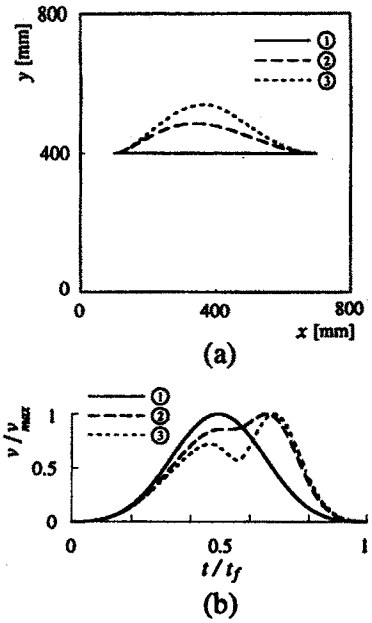

Fig.7 Generated trajectories with single-peaked and double-peaked velocity profiles

$(0.4,\ 0.7)^T$ [m], respectively. Also, t_i^a and t_i^b were set empirically with respect to the specified time t_f as follows: $t_x^a = t_y^a = 0.35t_f$, $t_\theta^a = 0.1t_f$, $|t_i^a - t_i^b| = \frac{t_f}{2}$. Figure 7 (b) shows the normalized velocity profiles for each generated spatial trajectory.

It can be observed from Fig. 7 that the generated curved spatio-trajectories have the double-peaked velocity profiles sinking around $t = \frac{t_f}{2}$. Also, as the amplitude of the curvature become to be larger, the velocity profile tends to be more sharply double-peaked. Owing to setting the via-point in the task space, the generated curved trajectories with double-peaked velocity profiles are in good agreement with the observed human trajectories.

5 Conclusions

In this paper, we focus on the task manipulating the holding nonholonomic car and try to generate human-like trajectories for the robots by imitating human generated trajectories. Via observation of the experiments with the subjects, we have found two human primitive velocity profiles: a single-peaked profile and a double-peaked one. Then, by applying the TBG based method, we could reproduce the spatio-temporal trajectories which have similar features of the observed human trajectories.

Future research will be directed to generate more complicated trajectories such as a trajectory including switching points by combining the primitive ones, and develop a motion planning method for a humanoid robot with consideration of arm geometrical constraints.

References

[1] K. Hirai, M. Hirose, Y. Haikawa and T. Takenaka: "The Development of Honda Humanoid Robot," in Proceedings of IEEE Int. Conf. on Robotics and Automation, pp. 1321–1326, 1998.

[2] P. Morasso: "Spatial control of arm movements," Experimental Brain Research, 42, pp. 223–227, 1981.

[3] T. Flash and N. Hogan: "The coordination of arm movements: An experimentally confirmed mathematical model," Biological Cybernetics, Vol. 57, pp. 1688–1703, 1985.

[4] Y. Uno, M. Kawato and R. Suzuki: "Formation and control of optimal trajectory in human multi-joint arm movement," Biological Cybernetics, Vol. 61, pp. 89–101, 1989.

[5] D. Bullock and S. Grossberg: "VITE and FLETE: Neural modules for trajectory formation and postural control," in Volitional Action (W. A. Hershberger, Ed.), pp. 253–297, Amsterdam, (Elsevier, North-Holland), 1989.

[6] P. Morasso, V. Sanguineti and T. Tsuji: "A dynamical model for the generator of curved trajectories," in Proceedings of the International Conference on Artificial Neural Networks, pp. 115–118, 1993.

[7] T. Tsuji, P. Morasso and M. Kaneko: "Feedback control of nonholonomic mobile robots using time base generator", in Proceedings of IEEE Int. Conf. on Robotics and Automation, pp. 1385–1390, 1995.

[8] T. Tsuji, P. Morasso, V. Sanguineti, and M. Kaneko: "Artificial Force-field based methods in Robotics," in Self-Organization, Computational Maps and Motor Control (P. Morasso and V. Sanguineti, Ed.), Advances in Psychology, 119, pp. 169-190, (Elsevier, North-Holland), 1997 .

[9] Y. Tanaka, T. Tsuji, M. Kaneko and Pietro G. Morasso: "Trajectory generation using Time Scaled artificial potential field," in Proceedings of IEEE/RSJ Int. Conf. on Intelligent Robots and Systems (1998) (To appear).

[10] D. A. Winter: "Biomechanics and motor control of human movement (2nd ed.)," Jhon Wiley and Son's Inc. , New York, pp. 41–43, 1990.

[11] M. Sampei and K. Furuta: "On time scaling for nonlinear systems: Application to linearization," IEEE Transactions on Automatic Control, Vol. 31, No. 5, pp. 459–462, 1986.

[12] C. Canudas de Witt and O.J.Sørdalen: "Exponential stabilization of mobile robots with nonholonomic constraints", IEEE Transactions on Automatic Control, Vol. 37, No. 11, pp. 1791–1797, 1992.